OXFORD

Cerebral Cortex, 2022, **32**, 4641–4656
https://doi.org/10.1093/cercor/bhab507
Advance access publication date 5 February 2022
Original Article

Multiscale functional connectome abnormality predicts cognitive outcomes in subcortical ischemic vascular disease

Mianxin Liu[1,†], Yao Wang[2,†], Han Zhang[1], Qing Yang[1], Feng Shi[3], Yan Zhou[2,*], Dinggang Shen[1,3,*]

[1]School of Biomedical Engineering, ShanghaiTech University, Shanghai 201210, China,
[2]Department of Radiology, Renji Hospital, School of Medicine, Shanghai Jiao Tong University, Shanghai 200127, China,
[3]Department of Research and Development, Shanghai United Imaging Intelligence Co., Ltd., Shanghai 200232, China

*Address correspondence to Dinggang Shen, School of Biomedical Engineering, ShanghaiTech University, Shanghai 201210, China.
Email: Dinggang.Shen@gmail.com. Yan Zhou, Department of Radiology, Renji Hospital, School of Medicine, Shanghai Jiao Tong University, Shanghai 200127, China.
Email: clare1475@hotmail.com
†These authors have contributed equally to this work

Subcortical ischemic vascular disease could induce subcortical vascular cognitive impairments (SVCIs), such as amnestic mild cognitive impairment (aMCI) and non-amnestic MCI (naMCI), or sometimes no cognitive impairment (NCI). Previous SVCI studies focused on focal structural lesions such as lacunes and microbleeds, while the functional connectivity networks (FCNs) from functional magnetic resonance imaging are drawing increasing attentions. Considering remarkable variations in structural lesion sizes, we expect that seeking abnormalities in the multiscale hierarchy of brain FCNs could be more informative to differentiate SVCI patients with varied outcomes (NCI, aMCI, and naMCI). Driven by this hypothesis, we first build FCNs based on the atlases at multiple spatial scales for group comparisons and found distributed FCN differences across different spatial scales. We then verify that combining multiscale features in a prediction model could improve differentiation accuracy among NCI, aMCI, and naMCI. Furthermore, we propose a graph convolutional network to integrate the naturally emerged multiscale features based on the brain network hierarchy, which significantly outperforms all other competing methods. In addition, the predictive features derived from our method consistently emphasize the limbic network in identifying aMCI across the different scales. The proposed analysis provides a better understanding of SVCI and may benefit its clinical diagnosis.

Key words: brain multiscale hierarchy; functional connectivity network; graph convolutional network; mild cognitive impairment; subcortical vascular cognitive impairment.

Introduction

Vascular cognitive impairment refers to a broad range of cognitive disorders pathologically attributing to impairments in the cerebral vascular system (Barbay et al. 2017). Subcortical vascular cognitive impairment (SVCI) induced by subcortical ischemic vascular disease (SIVD) is one of the commonest forms of vascular cognitive impairment (Beishon et al. 2017). The SVCI is defined as a continuum of cognitive impairment from an intermediate and reversible state, that is, mild cognitive impairment (MCI), to vascular dementia (VaD) (Skrobot et al. 2018). VaD has become the second major cause of dementia after Alzheimer's disease (AD) (Román 2002; Jia et al. 2020), which was recently reported to account for about 16% of all causes of dementia (Cao et al. 2020). There is also accumulating evidence that vascular pathology may play an important role in the development of AD (Beishon et al. 2017). Therefore, understanding SVCI could be crucial for preventing VaD and potentially helpful to a better understanding of AD.

Previous studies on SVCI focused on bridging the cognitive impairments to focal structural lesions exhibited in conventional magnetic resonance imaging (MRI) data (Roh and Lee 2014). The focal lesions associated with SVCI include lacunar infarct, white matter hyperintensity (WMH), perivascular space, cerebral microbleed, and brain atrophy. However, although being extensively studied, the dependency between the brain focal lesions and clinical manifestations in cognitive changes remains controversial and elusive (Duering et al. 2011; Biesbroek et al. 2013, 2017). The patients with significant and comparable brain lesions can either have no cognitive impairment (NCI) or exhibit subtyped MCI such as amnestic MCI (aMCI) and non-amnestic MCI (naMCI) (Ter Telgte et al. 2018).

Recent studies demonstrated the impacts of the focal lesions on the neural connectivity with diffusion tensor imaging (DTI) and found that focal lesions can influence the surrounding, even remote areas (Lawrence et al. 2014; Wang et al. 2017; Du et al. 2020). Parallel studies

Received: October 12, 2021. **Revised:** December 8, 2021. **Accepted:** December 9, 2021

explored the origin of variable cognitive performances under vascular pathology from the perspectives of brain functions (reviewed in Wang et al. 2020). Such effort also aimed to elucidate how the structural lesions impact neural functional interactions and further influence cognitive abilities (see review in Ye and Bai 2018). Functional MRI (fMRI) can indirectly monitor spontaneous neural activities by probing fluctuations in blood oxygen level-dependent (BOLD) signals. Defined by a brain atlas (brain region parcellation scheme), regional BOLD signals can be extracted and used to construct functional connectivity network (FCN) for investigating neural information exchanges as temporal synchronizations. Among the FCN-based studies, the abnormal connectivity within the default mode network (DMN), one of functional subnetworks relating to the high-level cognitions, has been regarded as a key factor reflecting the cognitive changes in SVCI patients (Sun et al. 2011; Yi et al. 2012; Zhou et al. 2016). Meanwhile, some other studies also showed that the abnormal functional connectivity due to SVCI could also be identified in multiple functional networks besides the DMN (Yi et al. 2015; Liu et al. 2019).

However, the existing FCN-based studies are still far from a conclusive understanding of SVCI, largely hindered by two major limitations.

First, previous FCN-based SVCI studies each utilized a specific parcellation atlas at a certain spatial scale to define brain regions for building the FCN. As the structural lesions induced by SIVD are heterogeneous in size, shape, and location (Ter Telgte et al. 2018), the single scale-based analysis may ignore impairments in functional interactions at the multiple spatial scales. For instance, microinfarcts are usually identified with a size of 50 μm in diameter, while WMHs can often be as large as a few cubic millimeters. Such a variation in the lesion size could lead to altered FCs among the brain regions across multiple spatial scales and induce variable cognitive outcomes. Therefore, using any specific brain parcellation at a fixed scale may only reveal the tip of the iceberg of the influence on the complex brain FC network. A multiscale FCN-based analysis can draw a more complete picture of the system-level pathological alternations in the brain with SVCI and thus could provide more accurate diagnosis. Besides, from the network neuroscience point of view, a single-scale analysis ignores the essential multiscale hierarchical organization of the brain system in both structure and functional dynamics (Van Essen and Felleman 1991; Betzel and Bassett 2017). Cortical parcellation studies have revealed that the brain functional regions at a coarse scale can be subdivided into subregions at finer scales (Hawrylycz et al. 2012; Schaefer et al. 2018) and the corresponding functional connectomes are multiscale, hierarchically organized in its nature. Such a multiscale hierarchy organization of brain connectomes have been regarded, by both theoretical modeling and empirical data analysis, crucial for efficient information processing in the brain. For example, it facilitates the flexibility for switching between information integration and segregation (Wang, Lin, et al. 2019a; Wang, Liu, et al. 2021b), and the sensitivity in the responses to external inputs (Liang et al. 2021). The multiscale FCN-based analysis on brains with SVCI, serving as a lesion model, could reveal more details on functional significances of multiscale FCNs during cognitive processes.

Second, it is noticeable that most of the abovementioned FCN-based SVCI studies typically used a group comparison or a correlational analysis as the main analysis methods. They could fail to exam out-of-sample generalizability of the revealed effects (Linden 2012; Whelan and Garavan 2014; Gabrieli et al. 2015; Lo et al. 2015). It is necessary to leverage the superiority of machine learning methods and prediction frameworks, which can sensitively identify generalizable diagnostic features (Fan et al. 2008; Jie et al. 2015). In the recent structural MRI-based SVCI studies, machine learning methods, especially deep learning, have already been adopted in identifications of SVCI patients. In our previous studies, we applied a convolutional neural network (CNN) to 3D fluid-attenuated inversion recovery (FLAIR) images and successfully classified different cognitive outcomes in SVCI patients, with above 90% accuracy in the out-of-sample data (Wang, Tu, et al. 2019b; Chen et al. 2020). However, in these works, CNN was used as a black box, where the interpretable features were not provided for further clarifications of the associations between brain and behavior changes. Meanwhile, deep learning methods have not been well explored in the FCN-based SVCI studies. Conventional deep learning methods cannot effectively extract the information encoded in the topological structure of the FCNs, because of its non-lattice-like graph structure. Attributing to the recent technology developments, the graph convolutional network (GCN) provides a promising solution to implement deep learning algorithms in the FCN-based SVCI studies. A GCN can learn feature representations from the FCN via, for example, message passing of nodal features based on graph Laplacian, preserving the topological information of FCN. This method has been successfully applied in the identifications of AD (Song et al. 2019; Wee et al. 2019), autism spectrum disorder (Parisot et al. 2018), attention-deficit/hyperactivity disorder (Saboksayr et al. 2020), and major depressive disorder (Jun et al. 2020). In addition, GCNs have demonstrated certain interpretability by highlighting predictive nodes (brain regions) and subnetworks (Li et al. 2020; Xing et al. 2021).

In order to fill the aforementioned gaps, in the present work, we hypothesize that the FC changes under SVCI can be more properly characterized from the FCNs at multiple spatial scales. To verify this hypothesis, we perform analysis to differentiate SIVD subjects with NCI, aMCI, and naMCI using multiscale FCN given by the pre-defined multiscale atlases, using both comparison-based and prediction-based frameworks. In addition, a novel GCN method is further proposed to differentiate

the cognitive outcomes (i.e., NCI, aMCI, or naMCI) more accurately in the SIVD patients based on the multiscale FCNs, with an ability of providing interpretable features for better understanding of the FCN changes under SVCI.

Materials and Methods

Ethics

The current study is approved by the Research Ethics Committee of Renji Hospital, School of Medicine, Shanghai Jiao Tong University, China. Written informed consents were obtained from all participants.

Participants

We investigate a total of 197 subjects (male/female = 151/46, ages at first scan = 50–84 years, right-handed), who were recruited from the outpatient clinic at the Neurology Department of Renji Hospital from July 2012 to January 2018. For each subject, we collected sociodemographic and clinical data, patient history, laboratory examinations, and conventional MRIs (see more details in Wang, Tu, et al. 2019b). Two experienced radiologists identified the SIVD by detecting WMH lesions as at least one lacunar infarct on the T2-FLAIR image (Galluzzi et al. 2005).

In line with our previous work (Wang, Tu, et al. 2019b), subjects with the following conditions are excluded: 1) cerebral hemorrhages, cortical and/or corticosubcortical non-lacunar territorial infarcts, and watershed infarcts; 2) specific causes of white matter lesions (e.g., multiple sclerosis, sarcoidosis, and brain irradiation); 3) other neurodegenerative diseases (including AD and Parkinson's disease); 4) signs of normal pressure hydrocephalus or alcoholic encephalopathy; 5) low education levels (<6 years); 6) severe depressions (Hamilton Depression Rating Scale $\geq$18), other psychiatric comorbidities, or severe cognitive impairments (inability to perform neuropsychological tests); 7) severe claustrophobia, and contraindications to MRI (e.g., pacemaker and metallic foreign bodies); 8) VaD (with diagnostic criteria described below).

Neuropsychological Assessment

The neuropsychological assessments for subjects were conducted within 2 weeks before or after MRI scans. The details of neuropsychological assessments can refer to our previous papers (Wang, Tu, et al. 2019b; Chen et al. 2020). In brief, a battery of neuropsychological tests is used to test multiple cognitive domains of participants, which covers attention, executive function, memory, language, and visuospatial function. In addition, the population distribution of the scores was constructed based on the scores for each measure of normal-aged people in Shanghai, China (Guo et al. 2007). The scores fallen beyond $\pm$1.5 standard deviations (SDs) from the mean are regarded as cognitive dysfunction. In addition, the VaD is identified as cognitive dysfunction in more than two cognitive domains with the abnormality in Lawton and Brody's Activities of Daily Living (ADL) Scale Test. MCI diagnosis is based on the following criteria: 1) ADL score should be normal or mildly impaired; 2) does not meet criteria for VaD; and 3) mild quantifiable cognitive impairment within one or more domains. The subjects who have suffered strokes or transient ischemic attacks between their assessments and MRI scans are excluded. Furthermore, the study also excludes the disable participants due to cognitive damages and motor sequelae using cognitive impairment histories and clinical judgments. Due to the lack of amyloid-β exams, MCIs induced by the mixed effects of vascular pathology and AD could not be fully excluded. The subtyping of MCIs followed the conventional Peterson/Winblad criteria (Winblad et al. 2004). NCI is identified by 1) detection of subcortical vascular disease and 2) the scores in all neuropsychological tests falling within the normal range ($\leq$1.5 SDs).

Based on the abovementioned assessments, the included SIVD patients are subdivided, based on their cognitive statuses, into subcortical vascular disease with NCI (81 subjects, with 96 longitudinal fMRI scans, male/female = 67/14, Mini-Mental State Exam [MMSE] = 28.6$\pm$1.3, Montreal Cognitive Assessment [MoCA] = 25.6 $\pm$2.6, and ages at first scan = 65.7$\pm$7.8 years) and subcortical vascular disease with MCI (116 subjects, with 125 fMRI scans). The MCI group is further divided into aMCI (59 subjects, with 64 fMRI scans, male/female = 43/16, MMSE = 27.1$\pm$2.1, MoCA = 21.2$\pm$3.4, and ages at first scan = 65.5$\pm$7.0 years) and naMCI (57 subjects, with 61 fMRI scans, male/female = 41/16, MMSE = 27.8$\pm$1.8, MoCA = 22.1$\pm$3.6, and ages at first scan = 64.8$\pm$7.1 years). We do not further classify the aMCI and naMCI into single-domain and multi-domain MCI due to the sample size limitation. There are no significant differences among NCI, aMCI, and naMCI groups in gender or age (Table 1).

MRI Protocol

MRI scan is performed using a SignaHDxt 3T MRI scanner (GE Healthcare, United States), with an eight-channel standard head coil with foam paddings to restrict head motions. The parameters of the echo-planar imaging sequence for the resting-state fMRI data collection are as follows: repetition time (TR) = 2000 ms, echo time (TE) = 24 ms, matrix = 64 × 64, flip angle = 90°, field of view (FOV) = 230 × 230 mm^2, slice thickness/gap = 4/0 mm, and number of slices = 34. The duration of the resting-state fMRI is 440 s (220 volumes). The sagittal T1-weighted images covering the whole brain were acquired by a 3D-fast spoiled gradient recalled echo sequence: TR = 5.6 ms, TE = 1.8 ms, matrix = 256 × 256, inversion time = 450 ms, flip angle = 15°, slice thickness/gap = 1/0 mm, number of slices = 156, gap = 0, and FOV = 256 × 256 mm^2.

fMRI Data Preprocessing

We adopt the standardized pipeline from the public available toolbox Data Processing Assistant for Resting-State fMRI (Yan and Zang 2010) in Matlab (Mathworks. R2020b) to preprocess the fMRI data. Each fMRI data undergo slice timing correction, head motion correction, nuisance

Table 1. Demographic and clinical statistics of the studied groups

		aMCI	naMCI
Gender	NCI	$\chi^2 = 1.96$, $P = 0.16$	$\chi^2 = 2.29$, $P = 0.13$
	aMCI		$\chi^2 = 0.01$, $P = 0.91$
		aMCI	naMCI
Age	NCI	$t = 0.18$, $P = 0.86$, CI = [−2.28, 2.75]	$t = 0.75$, $P = 0.46$, CI = [−1.60, 3.53]
	aMCI		$t = 0.56$, $P = 0.57$, CI = [−1.86, 3.33]
		aMCI	naMCI
MMSE	NCI	$t = 5.22$, $P < 0.01$, CI = [0.96, 2.12]	$t = 3.20$, $P < 0.01$, CI = [0.33, 1.41]
	aMCI		$t = -1.77$, $P = 0.08$, CI = [−1.42, 0.08]
		aMCI	naMCI
MoCA	NCI	$t = 8.31$, $P < 0.01$, CI = [3.41, 5.54]	$t = 6.27$, $P < 0.01$, CI = [2.41, 4.64]
	aMCI		$t = -1.33$, $P = 0.19$, CI = [−2.36, 0.47]

χ^2: the χ^2-statistics from chi-square test. t: the t-statistics from t-test. CI: 95% confidence interval for the difference in population means.

covariate regression, spatial normalization to the Montreal Neurological Institute space, temporal filtering, and spatially smoothing. Specifically, the nuisance covariates include head motions (ridge body with 6 degrees of freedom model), white matter signals, and cerebrospinal fluid signals. The spatial normalization is performed using Diffeomorphic Anatomical Registration Through Exponentiated Lie Algebra algorithm (Ashburner 2007) with the aid of T1-weighted images. And we apply a band-pass filter ($0.01 \leq f \leq 0.1$ Hz) for temporal filtering and a Gaussian kernel with full-width at half-maximum of $4 \times 4 \times 4$ mm^3 for spatial smoothing.

We then apply the multiscale brain parcellation atlases (Schaefer et al. 2018), which were generated by clustering the FC patterns of all brain gray matter voxels from 1489 participants based both on their local and global similarities. By tuning the resolution parameter in the clustering analysis, multiscale parcellations (from 100 ROIs to 1000 ROIs) were generated and were made publically available.[1] In the presented work, we use the atlases at the scales from 100 to 500 ROIs (Fig. 1A). The ROIs given by different parcellations at different scales preserve a similar structure of the seven resting-state functional networks (RSNs) defined by Yeo (Thomas Yeo et al. 2011). The spatial relationships among ROIs in these multiscale atlases can thus be regarded as a biologically meaningful brain hierarchy.

Based on one of these atlases, the FCN at a specific spatial scale can be built (Fig. 1B). At each scale P (with P ROIs), averaging the BOLD signals within voxels belonging to each ROI leads to the ROI signals, which are then pair-wise inter-correlated by Pearson correlation to generate the FCN at the scale P, called $\mathbf{FCN}_P$. We further regress out the effects of gender and age from each off-diagonal FC in the individual FCN to ensure the differences among groups barely depend on the effects of disease conditions.

[1] :https://github.com/ThomasYeoLab/CBIG/tree/master/stable_projects/brain_parcellation/Schaefer2018_LocalGlobal/Parcellations

Differentiating Power of Each RSN

Previous FCN-based works on SVCI reported that significant differences are detected in distinct RSNs (Ye and Bai 2018; Wang et al. 2020). We systematically test whether the detected differences are specific to a certain investigating scale or widely detectable at different scales. To do this, we conduct group-level statistical analysis on each FC link to identify significant group differences (P-value<0.01) in the FC links of each $\mathbf{FCN}_P$ at a certain scale P (we only check the upper triangle part of the FCN because the FC matrix is symmetry). The amount of the detected significant FC links is counted for intra-RSN connections of each RSN and inter-RSN connections between each pair of RSNs. Since the RSN size and the scale are both different, we further normalized the quantities of the intra- and inter-RSN FCs with group differences with respect to the possible numbers of the FC among the consisting RSNs under the fully connected condition at a certain scale. This leads to a comparable metric to evaluate distinct differentiating powers (DPs) among the 14 intra-RSN and 42 inter-RSN connections in both hemispheres as well as those at different scales when conducting paired group comparisons among NCI, aMCI, and naMCI.

Machine Learning Methods

Single Scale-Based Methods

Connectome-Based Prediction Model

Among the traditional machine learning-based study, the connectome-based prediction model (CPM) is a representative method (Shen et al. 2017; Sui et al. 2020). It initially uses brain–behavior correlations to select informative FCs as features and then uses these features to train a machine learning-based classifier (such as a support vector machine [SVM]) or a simple linear regression model to predict individual behaviors (Kristanto et al. 2020; Wang, Goerlich, et al. 2021a). We adopt this method as the baseline method.

With the CPM, we perform two steps to generate diagnostic predictions. First, the feature selection is

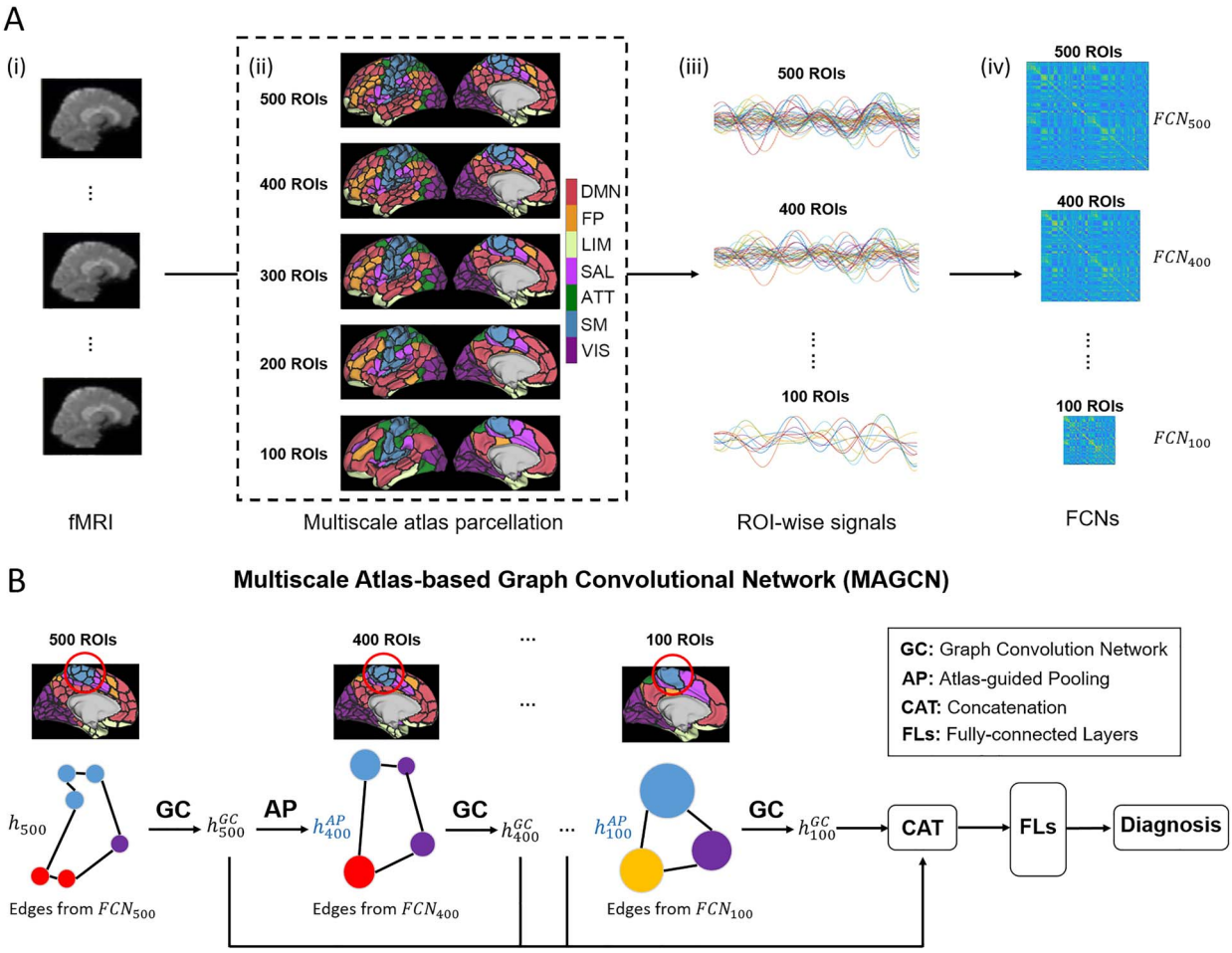

Figure 1. The schematic illustration of the main method. (A) The procedures to obtain multiscale FCNs. (i) the fMRI data from one individual is inputted and preprocessed. (ii) The application of the Schaefer's multiscale atlases to the fMRI data. The black border lines indicate boundaries of ROIs and the colors encode the resting-state network (RSN) to which the ROI belongs. The RSNs include DMN, frontoparietal network (FP), limbic network (LIM), salience network (SAL), attention network (ATT), somatomotor network (SM), and visual network (VIS). (iii) The extraction of ROI-averaged signals. (iv) The construction of multiscale FCNs from individual fMRI data. (B) The architecture for multiscale atlas-based GCN (MAGCN). The multiscale FCNs are extracted via a series of GCNs connected by the APs. The nodal features h are integrated with skip connections and concatenations, based on which individualized diagnosis is generated.

performed based on the P-values calculated from statistical comparison between two groups in the training set. The FCs with significant differences (at a P-value <0.05) are selected as features and used in both training and testing. Second, the selected features (connectivities) are vectorized and inputted to a SVM classifier. Different kernels for SVM are tested, including linear, polynomial, Gaussian, and Sigmoid, which leads to different results on the validation set. We report the best one among them. The other hyperparameters are kept as the default setting in the "SVC" function in the "*Scikit-learn*" package (Pedregosa et al. 2011).

Graph Convolutional Neural Network

The GCN can automatically abstract the feature representations for graph data by propagating the nodal features via graph Laplacian and further select features by applying an learned kernel on the features. Here, we choose the most prevalent version of GCN, namely spectral graph convolution (Defferrard et al. 2016; Kipf and Welling 2017). For a given adjacency matrix A and nodal features h, the graph convolution operation can be formulated in as:

$$h^{\mathrm{GC}} = \mathrm{GC}(A, h) = \sigma\left(\tilde{D}^{-\frac{1}{2}}\tilde{A}\tilde{D}^{-\frac{1}{2}}hW\right), \qquad (1)$$

where $\tilde{A} = A + I$, I is the identity matrix, $\tilde{D}$ is the corresponding degree matrix of $\tilde{A}$, W is the estimated kernel weight matrix, and $\sigma(\bullet)$ is a nonlinear activation function.

During implementation, we choose the ReLU function as the nonlinear activation function. An identity matrix is used as a nodal feature to let the GCN model focus on the topology of the FCN. The GCNs are attached with dropout functions (rate = 0.3), followed by two fully-connected layers (FLs). Each FL is associated with a batch normalization and a Rectified Linear Unit (ReLU) activation function. The outputs from the second FL are

normalized by a Softmax function to generate a predicted probability for two classes (Fig. 1B). These configurations for GCN and FL are kept consistent in all tested methods.

Multiscale-Based Methods

Classical Multiview Methods

To integrate multiscale features of the brain functional interactions, we apply two classical methods, namely "feature fusion" and "decision fusion." In the feature fusion, we train a model with multiple GCNs to independently process the FCNs at the different scales. The outputted features from these GCNs are combined by concatenation and further feed into FLs to generate predictions. We call this method **multiple GCNs (MGCN)**. Second, we choose **Majority Voting** as the representative method for decision fusion. We utilize GCN-based classifiers established in the independent trainings at the different scales and regard each of their predictions as one vote. These votes are pooled and counted, where the most voted class generates the final prediction of the whole model. During multi-classifications, under equally voted conditions (two of the three classes got equal votes since we used five scales), the model is forced to give prediction to the disease class (aMCI, or naMCI). Note that, in case of the aMCI-vs-naMCI classification with equal votes, the model's prediction is set to the aMCI class.

Multiscale Atlas-Based Graph Convolutional Neural Network

The Multiscale Atlas-Based Graph Convolutional Neural Network (MAGCN) is proposed in our previous paper (Liu et al. 2021), where the method is described in detail and systematically validated. Briefly, MAGCN extracts the features from multiscale FCNs by layers of GCNs and feature poolings following the hierarchical relationships defined in the multiscale atlases. First, an Atlas-guided Pooling (AP) operation is defined based on the spatial overlapping among ROIs defined by atlases at different scales (as illustrated in Fig. 1B). The AP operates on the node features defined by the atlas at scale P and converts them into the feature map for the atlas at scale Q ($P > Q$), based on the mapping matrix in the following form:

$$M_{\mathcal{R}\to\wp}(i,j) = \begin{cases} 1, & \rho > \mathbf{Th} \\ 0, & \text{Otherwise} \end{cases}, \qquad (2)$$

where the **Th** is a threshold applied to the overlapping ratio ρ, which is computed by the number of voxels of ROI i in the atlas at scale P that is spatially overlapping with ROI j in the atlas at scale Q divided by the total number of voxels of ROI i. For the results reported below, we use $\mathbf{Th} = 0$, which is consistent with our previous paper (Liu et al. 2021). Through a matrix multiplication with $M_{P\to Q}$, feature map h_P^{GC} defined at scale$P$ from GCN is pooled into a new feature map h_Q^{AP} defined at scale Q.

The MAGCN is then built by stacking GCNs and APs in a hierarchical manner (as shown in Fig. 1B). Each GCN is processing FCN at a specific scale with the inputs of nodal features from GCN at the neighboring finer scale (except that the first GCN uses identify matrix as the initial nodal feature input, that is, the h_{500} in Fig. 1B). The APs thus introduce inter-dependencies among the GCNs based on the hierarchy, which is expected to promote the feature representation process. The skip connections are further added into the architecture to enable the features from FCNs at different scales to jointly determine the final prediction. The joint feature is inputted into the two FLs to provide probabilistic predictions for two classes in bi-classification.

Feature Interpretability of MAGCN

To reveal the predictive features of deep learning methods in the NCI, aMCI, and naMCI classifications, we utilize the Gradient-guided Class Activation Map (Grad-CAM) algorithm proposed in the study of Selvaraju et al. (2017). In short, the Grad-CAM regards the gradient between prediction outputs and the feature maps at intermediate hidden layers of the deep neural network as the importance of features. It thus applies the gradient values to weight the elements in the feature maps, that is, the product between gradient map and feature map, namely the class activation map (CAM), which offers a visible map for spotting the predictive features. In this work, we detect the predictive brain regions with CAM.

In the analysis, we first compute the CAM of the disease group based on models from bi-classifications (in the aMCI-vs-naMCI classification, it is naMCI) for each individual from the models trained in the cross validations. Note that for a given individual, the CAMs from the two classes are anti-correlated. The results from the models are then weighted-averaged based on the AUCs, and the individual results are further averaged to obtain the group-wise CAM, with the patterns shown in Figure 4. We further coarse-grain the CAM patterns using the correspondences between ROIs and RSNs defined in the atlas, resulting in the statistics of RSN-wise averaged CAM values in Figure 5.

Experiments

Implementation

All the prediction algorithms are implemented in Python (Version 3.6.2). The SVM algorithm is based on the "SVC" function from "*Scikit-learn*" package (Pedregosa et al. 2011), while the neural network models are based on "*Pytorch*" framework (Paszke et al. 2019). The training parameters for neural network models are identically set as training epoch = 100, learning rate = 0.001, and batch size = 30. Adam (Kingma and Ba 2015) with a weight decay of 0.01 is used as an optimizer, and the weighted cross-entropy loss is adopted as the loss function. The weights are adaptively set by the inverse of the sample ratio in the training set. Other parameters of the neural network models are initialized with random weights. One Nvidia GTX 3080 GPU is used to accelerate the training.

Validation Scheme and Evaluation Metrics

Due to the existing longitudinal scans for the same subject, we design a special 5-fold cross-validation to evaluate the performance of the models. The subjects are assigned into the 5-folds with the same sample size, with 4-folds as the training set and the remaining 1-fold as the testing set. The roles of folds were exchanged till all folds played as testing set once. Each model is respectively trained and tested using different training–testing splits. We assign the fMRI scans according to the subject assignments, which ensures that no repeated scans from the same subject shall appear in both training and testing sets. Noted that the size of the image in each training and testing set can be different. Also, since the diagnosis may change at different longitudinal scans (e.g., NCI converts to aMCI), for each bi-classification, we exclude all the irrelevant longitudinal scans with diagnosis being not used in the classifications.

Under the sample imbalance, we choose four metrics from different aspects to evaluate the performance, that is, the accuracy (ACC), sensitivity (SEN), specificity (SPE), and area under the receiver operating characteristic curve (AUC). The means and SDs of the four performance metrics are calculated. For the multi-classification task, we assess the performance with overall ACC and the SENs for each class.

Statistical Analysis

To identify the difference at FCs among NCI, aMCI, and naMCI groups, two-sample *t*-tests are performed using the build-in function "*ttest2*" in Matlab (R2020b, Mathworks Inc, USA). The differences in age, MMSE, MoCA, and gender among the groups are tested using two-sample *t*-tests and chi-square tests with "*ttest2*" and "*chi2test*"[2] in Matlab. We also apply one-sided paired *t*-test with "*ttest*" in Matlab to measure if our proposed method significantly improve the diagnosis performance compared to the competing methods. When results are marginal significant ($0.05 \leq P \leq 0.10$), we provide the *P*-values and associated statistics for references. Note that a non-significant result ($P > 0.10$) may be due to either small improvement by MAGCN, or large variation in the results from either (or both) method(s).

Results

Variation of the RSNs' Differentiating Powers, across Multiple Scales, for SVCI

First, we explore whether the amount of the detected significant FC differences for intra- and inter-RSN connections had any interplay with the investigating spatial scale. The DPs for each intra- and inter-RSN connection is visualized in Figure 2*A*. The group differences as revealed by DPs are found distinctive depending on different RSNs with notable variation at different spatial scales. Along with the spatial scale changed, some connections (e.g., between the limbic and somatomotor [SM] networks in NCI vs. naMCI) keep showing high DPs, while others (e.g., between the limbic and frontoparietal (FP) networks in NCI vs. naMCI) have high DPs only at a certain scale. Such varying DPs from RSNs at multiple spatial scales suggest that the SVCI could exert distinct impacts on the FCNs at different spatial scales and that a scale specific study could only reveal one facet of such a complex influence.

Interestingly, in all the comparing conditions, intra-DMN subnetworks do not exhibit high DP. This phenomenon can be attributed to our normalization of subnetwork size. DMN has the largest size among all the RSNs in the used atlases (Schaefer et al. 2018), with its size increased along with the enlargement of scale. This leads to a higher chance to identify significant FCs in DMN. Indeed, in the unnormalized results (Fig. 2*B*), the connections between left and right DMNs are identified as the highest DP when comparing aMCI and naMCI. These findings suggest that the heterogeneity in network sizes and the size changes along scales could be important aspects that are commonly neglected in the previous studies when evaluating the cruciality of RSNs under SVCI.

More Accurate Diagnoses by Using Multiscale Hierarchical FCNs

The group comparison framework may not guarantee the generalizability of the revealed differences. We further demonstrate that the abnormalities in FCNs can be heterogeneous at different scales using the prediction framework. We apply two prediction methods, that is, CPM (with SVM as the classifier) and GCN, on NCI-vs-aMCI, NCI-vs-naMCI, and aMCI-vs-naMCI classifications. In Figure 3 and Tables 2–4, it can be observed that the single scale-based predictions exhibit distinct performances at different scales. For the CPM-based predictions, the scale with 500 ROIs is consistently identified as the optimal scale for NCI-vs-aMCI, NCI-vs-naMCI, and aMCI-vs-naMCI classifications. And, for the GCN-based analysis, the 200-ROI scale can be regarded as the optimal scale for these three classification tasks. These observations are again consistent with the above interpretation that the SVCI-related FCN alternations could diverge when investigating different scales. In addition, the SVM-based CPMs generally yield values from 50% to 60% in all metrics, while the GCN-based predictions achieve values in a range from 65% to 70%, suggesting advantages of the GCN-based FCN processing over the SVM-based CPM.

We then test three multiscale-based classification methods, including our proposed method (MAGCN). First, all multiscale-based methods yield higher performance than single scale-based methods in terms of ACC and AUC (Fig. 3 and Tables 2–4). This indicates the effectiveness of the joint analysis using multiscale FCNs. Since disease-related changes are separately identified at multiple scales, our result suggests that it is crucial to

[2] https://www.mathworks.com/matlabcentral/fileexchange/16177-chi2test

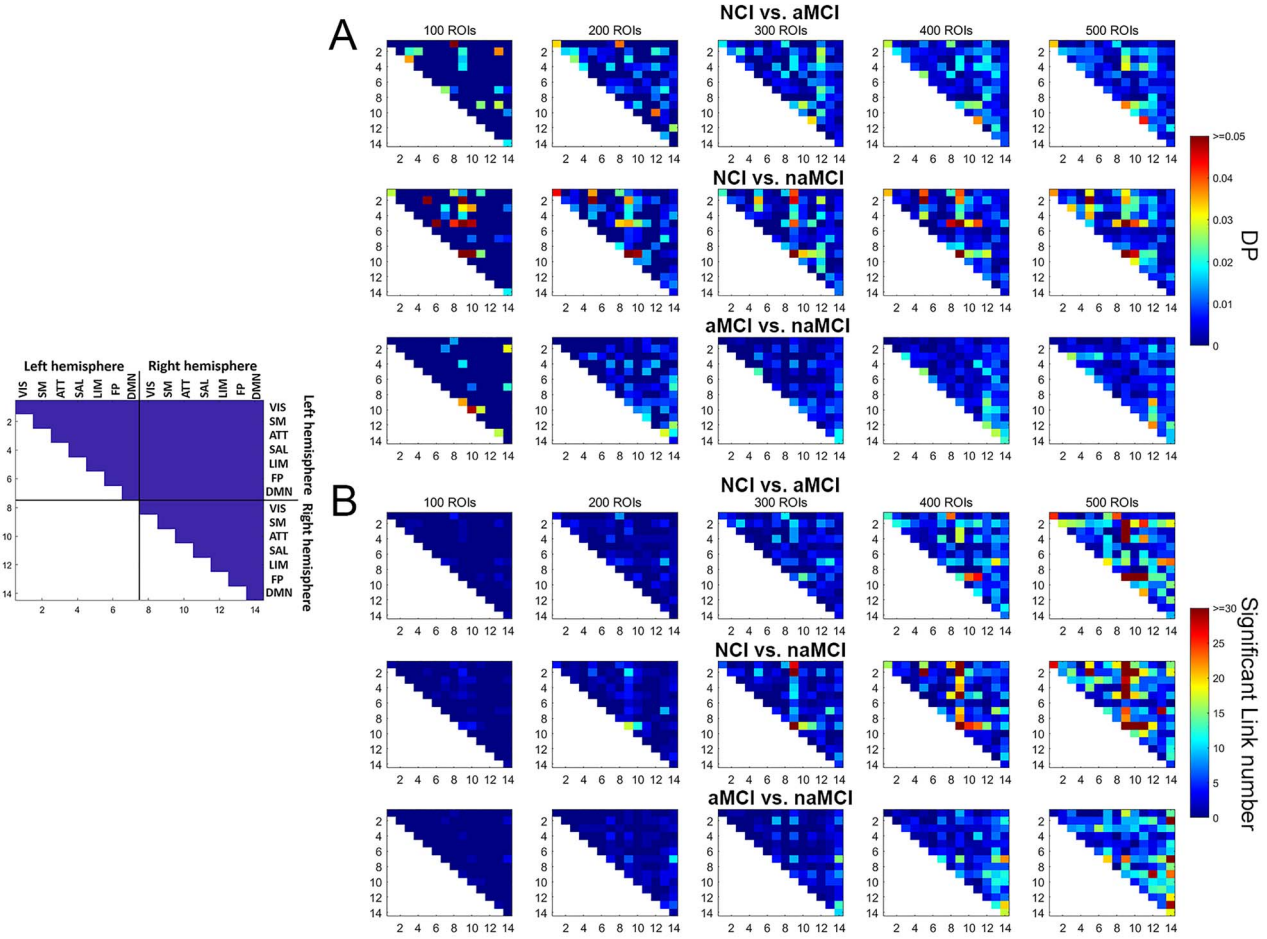

Figure 2. Different DPs of the intra- and inter-RSN connections at different scales, when conducting pairwise group comparisons among NCI, aMCI, and naMCI. For comprehensive illustrations, we show both DPs (a normalized metric, with respect to the RSN sizes at a certain scale) in (*A*) and the non-normalized metrics (i.e., the original number of the FC links with significant group differences) in (*B*). Networks 1–7 and 8–14 represent the seven RSNs in the left and right hemispheres, respectively. Only the upper triangle of the connectivity matrix is presented since the matrix is symmetric.

combine all those different-scale features to obtain accurate diagnosis. In addition, in all three bi-classifications, our proposed method MAGCN obtains higher performances over the simple feature-fusion and decision-fusion methods on three of the four metrics, where 11 out of the 18 pairs of comparisons show significances or marginal significances (Tables 2–4). We further conduct a NCI-vs-aMCI-vs-naMCI multi-classification using GCN-based and multiscale-based methods (Table 5). The changing trends of the performances are akin to those under the bi-classification scenarios. This supports the effectiveness of MAGCN in integrating distributed information at different scales based on the priors of the brain hierarchy. Note that the feature-fusion and decision-fusion methods "independently" consider the information at multiple scales, while the MAGCN introduces the inter-scale dependencies during the feature extraction and leverages the hierarchically refined features in the classification stage. Such a better performance of the MAGCN may also indicate that the SVCI could influence multiscale FCNs in a cascaded manner.

Diagnostic Features in MAGCN Emerged in Multiple RSNs at Multiple Scales

The predictive features encoded inside the MAGCN are explored using Grad-CAM (see Materials and Methods). The spatial patterns of the feature importances (i.e. predictabilities) are offered in Figure 4, and the RSN-wise distributions are depicted in Figure 5. In Figure 5A, we can first note that the limbic network (LIM) exhibits the highest predictability for differentiating aMCI from NCI at almost all investigated scales (100–400 ROIs). It could be reasonable that LIM is the most predictive for the amnestic impairment because the memory abilities are associated with the LIM (refer to the orbitofrontal cortex and temporal pole according to the atlas) (Frey and Petrides 2002; Smith and Kosslyn 2006; Barbey et al. 2011; Farovik et al. 2015). In addition, DMN is regarded as the second predictive RSN at the 200- and 400-ROI scales. However, for the identification of naMCI from NCI, the predictive features are contributed by different RSNs at multiple scales, that is, FP at 100-ROI scale, SM at 200-ROI scale, DMN at 300-ROI scale, and salience (SAL) networks at 400- and 500-ROI scales (Fig. 5B). To separate

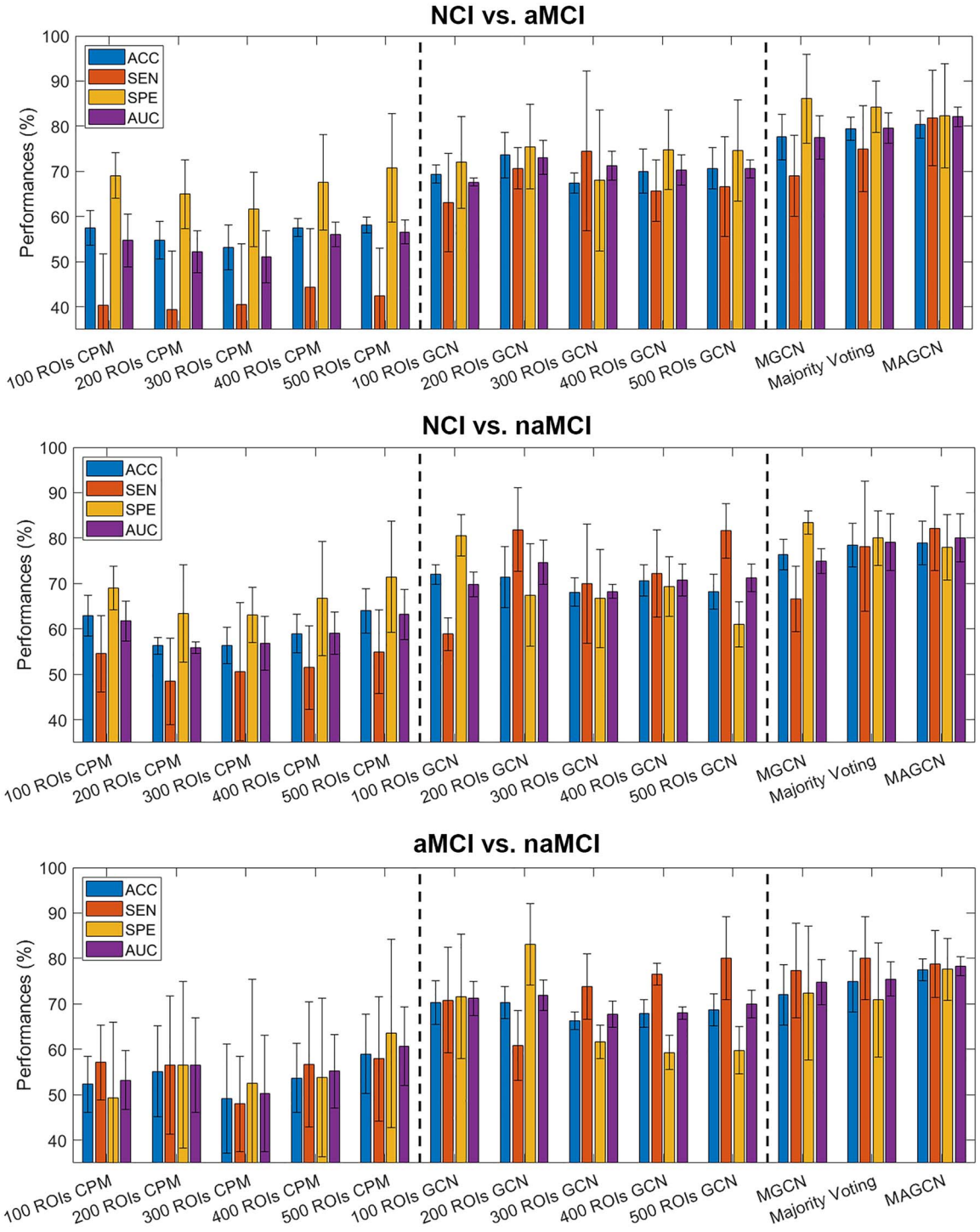

Figure 3. Classification performances shown as bars along with error plots.

aMCI and naMCI, although the features from LIM are still regarded as crucial, other RSNs are contributing to classifications more remarkably (Fig. 5C), which matches the observations in Fig. 5A,B. At the 300- and 500-ROI scales, DMN is ranked as the top predictive RSN in NCI-vs-naMCI and aMCI-vs-naMCI classifications, respectively. However, DMN does not consistently show importances during the prediction when the parcellation scale is altered.

Discussion

Dysfunction in Multiple Scales Not Single Scale

We first demonstrate that the differentiating features emerged at multiple scales of the brain functional communications. The investigation scale could be crucial when evaluating the predictability of RSNs. Comparing to the independent analysis at each scale, joint analysis to integrate all these features provides a better way of predicting clinical cognitive outcomes under SIVD. Our

Table 2. The results of NCI-vs-aMCI classifications

	Method	ACC	SEN	SPE	AUC
Single scale-based methods	100 ROIs CPM	57.5±3.9**	40.4±11.4**	69.1±5.1*	54.7±5.9**
	200 ROIs CPM	54.8±4.2**	39.4±13.0**	65.0±7.6[a]	52.2±4.7**
	300 ROIs CPM	53.2±5.0**	40.6±13.4*	61.6±8.3*	51.1±5.8**
	400 ROIs CPM	57.5±2.0**	44.3 ±13.1*	67.6±10.6[b]	56.0±2.7**
	500 ROIs CPM	58.1 ±1.8**	42.4±10.6**	70.8 ±12.0[c]	56.6 ±2.6**
	100 ROIs GCN	69.4±2.0**	63.1±10.9*	72.0±10.2	67.6±0.9**
	200 ROIs GCN	73.6 ±5.0*	70.7±4.6*	75.5 ±9.3	73.1 ±3.8*
	300 ROIs GCN	67.4±2.2**	74.5 ±17.7	68.0±15.6*	71.2±3.2**
	400 ROIs GCN	70.0±4.9**	65.7±6.8*	74.8±8.8	70.3±3.4**
	500 ROIs GCN	70.7±4.6*	66.6±11.0[d]	74.6±11.2	70.6±2.0*
Multiscale-based methods	MGCN	77.6±5.1[e]	69.0±9.0*	**86.1** ±9.8	77.5±4.8*
	Majority Voting	79.4±2.6	75.0±9.5[f]	84.3±5.7	79.6±3.3[g]
	MAGCN	**80.4** ±3.0	**81.8** ±10.6	82.3±11.5	**82.1** ±2.2

The mean and SD of performance in each cross-validation are reported (in %). The underlines indicate the best performances among scales using the same single-scale based methods. The bolds highlight the best performances among all the methods. *: MAGCN has a significantly higher performance than the competing method at $P<0.05$ level. **: $P<0.01$. [a]: MAGCN shows marginal significant improvement over this result, with $t=2.09$, $P=0.05$, CI = $[-0.3, +\infty]$. [b]: $t=1.98$, $P=0.06$, CI = $[-1.1, +\infty]$. [c]: $t=1.89$, $P=0.07$, CI = $[-1.5, +\infty]$. [d]: $t=1.75$, $P=0.07$, CI = $[-3.3, +\infty]$. [e]: $t=1.59$, $P=0.09$, CI = $[-0.8, +\infty]$. [f]: $t=1.49$, $P=0.10$, CI = $[-3.0, +\infty]$. [g]: $t=1.83$, $P=0.07$, CI = $[-0.4, +\infty]$.

Table 3. The results of NCI-vs-naMCI classifications

	Method	ACC	SEN	SP-	AUC
Single scale-based methods	100 ROIs CPM	62.9±4.5**	54.6±8.4**	69.0±4.8*	61.8±4.4**
	200 ROIs CPM	56.3±1.8**	48.5±9.5**	63.4±10.7*	55.9±1.3**
	300 ROIs CPM	56.3±4.0**	50.6±15.2**	63.1±6.1**	56.9±5.9**
	400 ROIs CPM	59.0±4.3**	51.5±9.2**	66.7±12.5[a]	59.1±4.7**
	500 ROIs CPM	64.0 ±4.9**	55.0 ±9.2**	71.5 ±12.2[b]	63.2 ±5.5**
	100 ROIs GCN	72.0 ±2.2*	58.9±3.6**	80.6 ±4.6	69.8±2.7*
	200 ROIs GCN	71.4±6.7	81.9 ±9.2	67.5±11.3	74.7 ±4.9
	300 ROIs GCN	68.1±3.1**	70.0±13.1[c]	66.7±10.8[d]	68.3±1.6**
	400 ROIs GCN	70.7±3.4*	72.2±9.6	69.3±6.6[e]	70.8±3.5*
	500 ROIs GCN	68.2±3.9*	81.6±6.0	61.0±4.9**	71.3±3.0*
Multiscale-based methods	MGCN	76.4±3.3*	66.6±7.2*	**83.4** ±2.6	75.0±2.7*
	Majority Voting	78.4±4.8	78.2±14.3	80.0±6.0	79.1±6.3
	MAGCN	**79.0** ±4.8	**82.2** ±9.3	78.0±7.2	**80.1** ±5.3

*: MAGCN has a significantly higher performance than the competing method at $P < 0.05$ level. **: $P < 0.01$. [a]: MAGCN shows marginal significant improvement over this result, with $t=1.99$, $P=0.06$, CI = $[-0.8, +\infty]$. [b]: $t=1.77$, $P=0.07$, CI = $[-1.3, +\infty]$. [c]: $t=1.62$, $P=0.09$, CI = $[-3.9, +\infty]$. [d]: $t=1.59$, $P=0.09$, CI = $[-3.8, +\infty]$. [e]: $t=1.61$, $P=0.09$, CI = $[-2.8, +\infty]$.

Table 4. The results of aMCI-vs-naMCI classifications

	Method	ACC	SEN	SPE	AUC
Single scale-based methods	100 ROIs CPM	52.3±6.1**	57.1±8.2*	49.4±16.5**	53.2±6.5**
	200 ROIs CPM	55.1±10.0**	56.6±15.2*	56.6±18.3*	56.6±10.4**
	300 ROIs CPM	49.1±12.0**	48.0±10.5**	52.6±22.8*	50.3±12.8**
	400 ROIs CPM	53.7±7.6**	56.7±13.8*	53.8±17.5*	55.2±8.1**
	500 ROIs CPM	59.0 ±8.7**	57.9 ±13.7**	63.5 ±20.8	60.7 ±8.7**
	100 ROIs GCN	70.3 ±4.8*	70.8±11.6*	71.6±13.7[a]	71.2±3.8*
	200 ROIs GCN	70.3 ±3.5*	60.8±7.7*	83.1 ±9.0	71.9 ±3.4*
	300 ROIs GCN	66.3±2.0**	73.8±7.2	61.6±3.7**	67.7±2.9**
	400 ROIs GCN	67.9±3.0**	76.6±2.4	59.3±3.8**	68.0±1.4**
	500 ROIs GCN	68.7±3.5**	80.1 ±9.1	59.8±5.2**	70.0±3.1**
Multiscale-based methods	MGCN	72.0±6.7[b]	77.3±10.4	72.4±14.7	74.8±5.0[c]
	Majority Voting	75.0±6.7	**80.1** ±9.1	70.9±12.6[d]	75.5±3.7
	MAGCN	**77.5** ±2.4	78.8±7.4	**77.6** ±6.8	**78.3** ±2.1

*: MAGCN has a significantly higher performance than the competing method at $P < 0.05$ level. **: $P < 0.01$. [a]: MAGCN shows marginal significant improvement over this result, with $t=1.59$, $P=0.09$, CI = $[-2.1, +\infty]$. [b]: $t=2.02$, $P=0.06$, CI = $[-0.3, +\infty]$. [c]: $t=2.04$, $P=0.06$, CI = $[-0.2, +\infty]$. [d]: $t=1.57$, $P=0.09$, CI = $[-2.5, +\infty]$.

proposed MAGCN that integrates the features following the brain hierarchy further boosts the classification performances. The results suggest that, under SVCI, the brain vessel pathology induces focal lesions and further have impacts on the efficiency of the brain functional communications at varying spatial scales. The results also show the clinical significance of investigating atypical configurations in multiscale hierarchical brain connectomes. This could be a general principle beyond the context of SVCI. Existing studies found that normal brain

Table 5. The results of NCI-vs-aMCI-vs-naMCI classifications

	Method	ACC_all	SEN_NCI	SEN_aMCI	SEN_naMCI
Single scale-based methods	100 ROIs GCN	46.7±2.7**	46.3±10.5*	49.1±11.7	48.0±4.7
	200 ROIs GCN	49.7±4.3*	55.1±8.3*	41.0±6.8*	52.9±6.6
	300 ROIs GCN	44.5±3.2**	42.2±7.4**	40.6±6.5*	55.3±12.7
	400 ROIs GCN	46.7±2.9**	50.9±9.1*	45.6±9.1	44.7±8.2
	500 ROIs GCN	50.2±5.5*	48.5±10.7*	51.4±14.4	51.3±8.6
Multiscale-based methods	MGCN	54.9±3.8	57.7±7.1	50.8±6.9	56.2±5.8
	Majority Voting	56.5±6.6	57.5±13.8	**55.4** ±11.4	**59.9** ±7.5
	MAGCN	**58.3** ±2.4	**67.2** ±10.1	50.2±5.3	52.2±13.5

*: MAGCN has a significantly higher performance than the competing method at $P < 0.05$ level. **: $P < 0.01$.

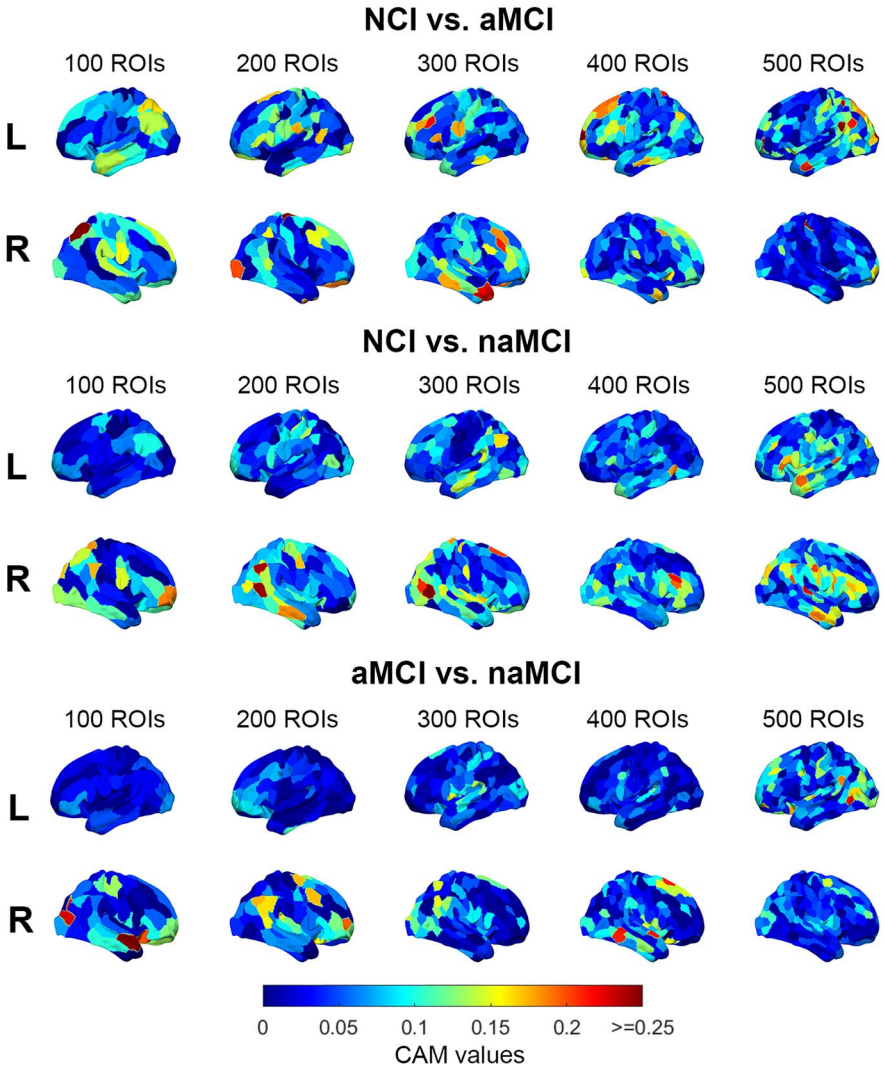

Figure 4. The multiscale spatial patterns of predictive features.

functional and structural connectomes exhibit different topological characteristics, such as degree distribution and small worldness, at different scales (Wang et al. 2009; Zalesky et al. 2010). This implies that the connectomes at distinct scales may reflect non-overlapping aspects of the brain information processing, although connectomes are correlated along the brain hierarchy. There are also accumulating evidence showing that the normal aging or disease could modify functional interactions intra- or inter-scales (Betzel et al. 2015; Zhang et al. 2017). For example, Betzel et al. (2015) illustrated that the investigated scale could have an impact on the association between the segregation of communities in FCN and the age effects. Zhang et al. (2017) observed that the intra- and inter-scale brain functional interactions in the hierarchical FCN, measured by so-called associated high-order functional connectivity, could be more informative than the single-scale FCNs in the MCI identification. These converging evidences demonstrate the functional significance of multiscale

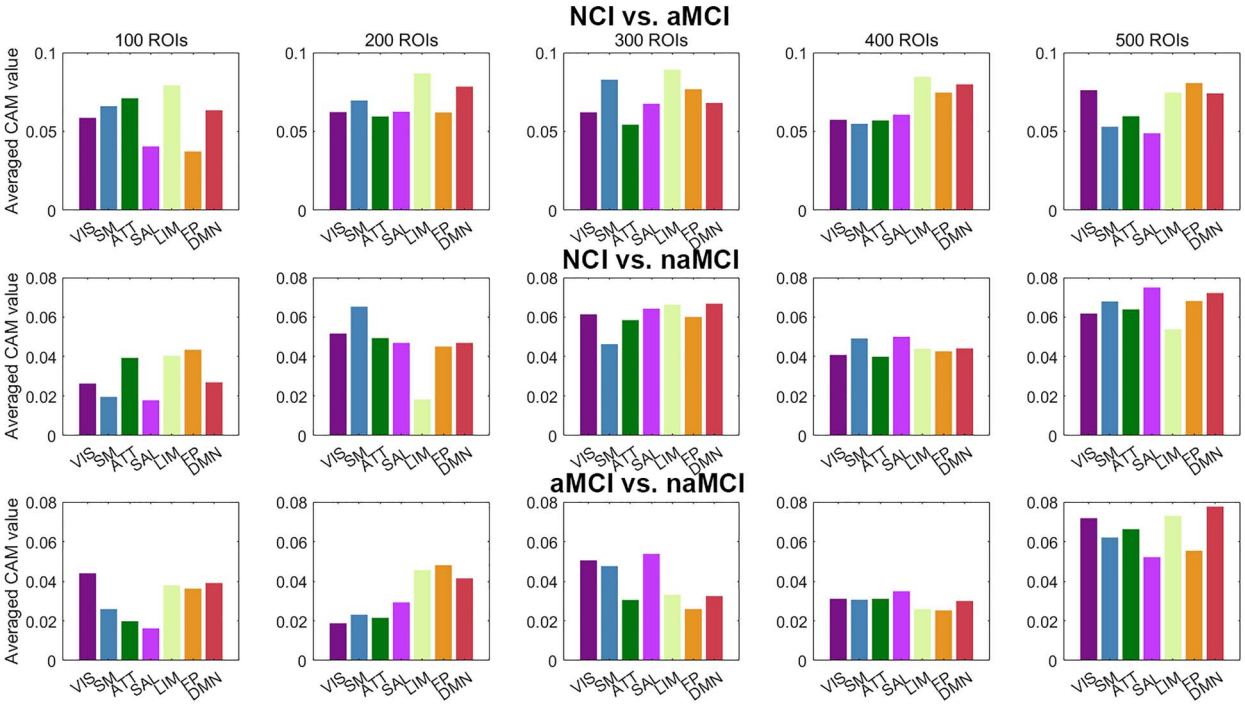

Figure 5. The RSN-wise distributions of predictive features from the MAGCN.

hierarchical connectomes underlying the cognitive processing.

Backing to SVCI, an interesting question to be further explored is the mechanism of how different structural lesions under SIVD associate with FC abnormalities across different spatial scales. One possibility is that different types of structural lesions could impact on white matter fibers at scales corresponding to their sizes and separately induce consequences on FCs at multiple scales. Another scenario can be that the focal lesion could affect the hubs shared by multiscale structural and functional networks and thus simultaneously influence connections at different scales. Also, since we do not compare NCI to healthy control group, it is also unknown whether the multiscale FCNs could provide alternative information pathways and thus underlie the reserve and compensatory mechanisms to protect the NCI subjects from cognitive impairments (Stern 2009; Brickman et al. 2011). In principle, when failures only occur in FCs at specific scales, the functional information exchanges could still be maintained by FCs at other scales and thus the cognitive ability remains normal. And here we observe that aMCI are associated by dysfunctions in limbic networks across several scales, which may offer indirect evidences to support the roles of multiscale FCNs in the brain reserve. Answering these two key questions could offer a whole picture of how the structural lesions influence neural dynamics and lead to cognitive impairment.

Dysfunction in Multiple RSNs Not Single RSN

Previous fMRI-based SVCI studies highlighted DMN as an important RSN being influenced by pathological factors and relating to cognitive impairments. However, some studies also reported that the FC abnormalities distribute in different RSNs besides DMN, including dorsal attention network, central-executive network, somatomotor network, and visual network (Ye and Bai 2018; Wang et al. 2020). The distributed abnormality involving multiple RSNs, favored by our results, can be reasonable since brain structural lesions are widely distributed in the brain (Wang et al. 2017; Qiu et al. 2021) and some of them demonstrate both local and remote impacts on brain connectivity. Therefore, it could be more natural to expect that the SCVI cannot be barely associated with DMN, but a joint of multiple RSNs. The observation can also deeply rooted into the complex nature of the MCI in cognitive symptoms. Previous SVCI studies highlighting DMN did not separately explore aMCI and naMCI, but treated MCI as an entire symptom (Sun et al. 2011; Yi et al. 2012; Zhou et al. 2016). However, the subtyping of the MCI reveals that the cognitive impairment can cover single and multiple cognitive domains, involving memory, executive functions, attention, and visuospatial ability or language (Petersen 2000; del Carmen et al. 2017). Therefore, when associating with multiple cognitive domains, the MCIs are less likely to be explained by a single RSN.

Pathology and Etiology behind aMCI and naMCI

Our results detect the limbic network and DMN as crucial indicators for aMCI under SIVD. Coincidently, these RSNs are also considered to be most pronouncedly damaged under AD (Van Hoesen et al. 2000; Zhang et al. 2010; Dhikav et al. 2014; Berron et al. 2020; Liang et al. 2021).

On the contrary, for naMCI, there is few RSN being consistently highlighted during the prediction.

Although AD-related effects are not completely excluded due to the lack of PET scans, these results may still indicate a potentially overlapping pathology between aMCI and AD, there is less similarity between naMCI and AD, in patients with SIVD. Consistently, previous clinical records found that aMCI (single- or multi-domain) is more related to a degenerative etiology and more likely to develop into AD dementia, while naMCI tends to originate from other etiology and to develop into non-AD dementia (Salvadori et al. 2016). From the perspective of clinical applications, our findings again deliver a clear message that differential clinical cares and treatments for different MCI subtypes could be important and might benefit to the prognosis. In addition, if the progression of aMCI under SIVD involves degenerative etiology besides vascular etiology, aMCI could serve as a clinical model to explore the interplays between vascular pathology and AD factors and elucidate the mechanism under the conversion from SVCI to AD (Beishon et al. 2017).

Deep Learning towards a More Precise SVCI Diagnosis

From the methodology viewpoint, our results also emphasize that the deep learning methods (GCN, MAGCN) have advantages in processing FCN over the classical machine learning methods, with the SVM-based CPM as a representative. The CPM performs the feature selection by comparisons under linear assumptions and uses a collection of the selected FCs in the subsequent prediction. However, features may not be properly selected using linear relationships, and the topological structure can be diminished by such "masking" using the *P*-values from group comparisons. In contrast, the GCN preserves the topological structure and automatically learns more suitable representations to abstract features from the entire FCN with better tackling on the nonlinearity, resulting in better performances in the subsequent prediction. Noticeably, the GCN is a general architecture that can be used in the processing of other graph data, such as the structural networks from DTI and dynamic FCN (Liu et al. 2021; Chen et al. 2017). The development of advanced GCN-based analysis could be promising to assist the diagnosis of SVCI and more other brain diseases.

However, we would like to indicate that our current deep learning model is still not robust to meet clinical demands, due to the use of limited sample. Further increase of the data size, for example, through multicenter collaborations, and systematic external validations on the methods could essentially push our deep learning model towards clinical applications.

Conclusion

In this work, we investigate the differences among NCI, aMCI, and naMCI using FCNs from multiple spatial scales and develop a novel automatic diagnosis algorithm. First, the results from single scale-based analyses clearly suggest that the disease-related information carried on FCNs is scale-dependent. Second, the joint multiscale analysis is beneficial for the diagnosis of SVCI, and multiscale features are thus complementary to each other. Third, our proposed MAGCN is able to more effectively integrate the distributed information at different scales based on the brain hierarchy and provide more accurate classifications among NCI, aMCI, and naMCI groups. Finally, the predictive features by MAGCN are located distributedly in RSNs, further showing variations across the investigating scales. Among all located RSNs at different scales, the limbic network is consistently regarded as crucial for identifying aMCI, indicating its FC deficits across all scales. To the best of our knowledge, we are the first to apply the GCN method to analyze FCNs from multiscale atlases for the SVCI study.

Overall, the results provide novel insights about SVCI and emphasize that the brain is a multiscale hierarchical complex system with distributed information processing based on interactions among functional subsystems (Colom et al. 2006; Gläscher et al. 2010). Under the atypical state, the pathology could be more properly characterized in the multiscale brain system, rather than a single RSN at a chosen scale.

Funding

National Natural Science Foundation of China (grant number 62131015); Science and Technology Commission of Shanghai Municipality (STCSM) (grant number 21010502600); ShanghaiTech Startup funds, the National Key Scientific Instrument Development Program (grant number 82027808); National Natural Science Foundation of China (grant number 82171885, 82001457, and 81901693); Shanghai Science and Technology Committee Project (Natural Science Funding: grant number 20ZR1433200; Explorer Program: grant number 21TS1400700); Shanghai Rising Stars of Medical Talent Youth Development Program, Youth Medical Talents-Medical Imaging Practitioner Program (grant number SHWRS(2020)_087).

Notes

Conflict of Interest: None declared.

References

Ashburner J. 2007. A fast diffeomorphic image registration algorithm. *NeuroImage*. 38:95–113.

Barbay M, Taillia H, Nedelec-Ciceri C, Arnoux A, Puy L, Wiener E, Canaple S, Lamy C, Godefroy O, Roussel M. 2017. Vascular cognitive impairment: advances and trends. *Rev Neurol (Paris)*. 173:473–480.

Barbey AK, Koenigs M, Grafman J. 2011. Orbitofrontal contributions to human working memory. *Cereb Cortex*. 21:789–795.

Beishon L, Haunton VJ, Panerai RB, Robinson TG. 2017. Cerebral hemodynamics in mild cognitive impairment: a systematic review. *J Alzheimers Dis*. 59:369–385.

Berron D, van Westen D, Ossenkoppele R, Strandberg O, Hansson O. 2020. Medial temporal lobe connectivity and its associations with cognition in early Alzheimer's disease. *Brain*. 143:1233–1248.

Betzel RF, Bassett DS. 2017. Multi-scale brain networks. *NeuroImage*. 160:73–83.

Betzel RF, Mišić B, He Y, Rumschlag J, Zuo X-N, Sporns O. 2015. Functional brain modules reconfigure at multiple scales across the human lifespan. *arXiv*. 1510:1–56.

Biesbroek JM, Kuijf HJ, van der Graaf Y, Vincken KL, Postma A, Mali WPTM, Biessels GJ, Geerlings MI. 2013. Association between subcortical vascular lesion location and cognition: a voxel-based and tract-based lesion-symptom mapping study. The SMART-MR Study. *PLoS One*. 8:e60541.

Biesbroek JM, Weaver NA, Biessels GJ. 2017. Lesion location and cognitive impact of cerebral small vessel disease. *Clin Sci*. 131: 715–728.

Brickman AM, Siedlecki KL, Muraskin J, Manly JJ, Luchsinger JA, Yeung LK, Brown TR, DeCarli C, Stern Y. 2011. White matter hyperintensities and cognition: testing the reserve hypothesis. *Neurobiol Aging*. 32:1588–1598.

Cao Q, Tan CC, Xu W, Hu H, Cao XP, Dong Q, Tan L, Yu JT. 2020. The prevalence of dementia: a systematic review and Meta-analysis. *J Alzheimers Dis*. 73:1157–1166.

del Carmen D-MM, García-Herranz S, Rodríguez-Fernández R, Venero C, Peraita H. 2017. Problems in classifying mild cognitive impairment (MCI): one or multiple syndromes? *Brain Sci*. 7:111.

Chen X, Zhang H, Zhang L, Shen C, Lee SW, Shen D. 2017. Extraction of dynamic functional connectivity from brain grey matter and white matter for MCI classification. *Hum Brain Mapp*. 38: 5019–5034.

Chen Q, Wang Y, Qiu Y, Wu X, Zhou Y, Zhai G. 2020. A deep learning-based model for classification of different subtypes of subcortical vascular cognitive impairment with FLAIR. *Front Neurosci*. 14:557.

Colom R, Jung RE, Haier RJ. 2006. Distributed brain sites for the g-factor of intelligence. *NeuroImage*. 31:1359–1365.

Defferrard M, Bresson X, Vandergheynst P. 2016. Convolutional neural networks on graphs with fast localized spectral filtering. *Adv Neural Inf Process Syst*. 29:3844–3852.

Dhikav V, Sethi M, Anand KS. 2014. Medial temporal lobe atrophy in Alzheimer's disease/mild cognitive impairment with depression. *Br J Radiol*. 87:20140150.

Du J, Zhu H, Zhou J, Lu P, Qiu Y, Yu L, Cao W, Zhi N, Yang J, Xu Q et al. 2020. Structural brain network disruption at preclinical stage of cognitive impairment due to cerebral small vessel disease. *Neuroscience*. 449:99–115.

Duering M, Zieren N, Hervé D, Jouvent E, Reyes S, Peters N, Pachai C, Opherk C, Chabriat H, Dichgans M. 2011. Strategic role of frontal white matter tracts in vascular cognitive impairment: a voxel-based lesion-symptom mapping study in CADASIL. *Brain*. 134: 2366–2375.

Fan Y, Gur RE, Gur RC, Wu X, Shen D, Calkins ME, Davatzikos C. 2008. Unaffected family members and schizophrenia patients share brain structure patterns: a high-dimensional pattern classification study. *Biol psychiatry*. 63:118–124.

Farovik A, Place RJ, McKenzie S, Porter B, Munro CE, Eichenbaum H. 2015. Orbitofrontal cortex encodes memories within value-based schemas and represents contexts that guide memory retrieval. *J Neurosci*. 35:8333–8344.

Frey S, Petrides M. 2002. Orbitofrontal cortex and memory formation. *Neuron*. 36:171–176.

Gabrieli JDE, Ghosh SS, Whitfield-Gabrieli S. 2015. Prediction as a humanitarian and pragmatic contribution from human cognitive neuroscience. *Neuron*. 85:11–26.

Galluzzi S, Sheu CF, Zanetti O, Frisoni GB. 2005. Distinctive clinical features of mild cognitive impairment with subcortical cerebrovascular disease. *Dement Geriatr Cogn Disord*. 19: 196–203.

Gläscher J, Rudrauf D, Colom R, Paul LK, Tranel D, Damasio H, Adolphs R. 2010. Distributed neural system for general intelligence revealed by lesion mapping. *Proc Natl Acad Sci U S A*. 107: 4705–4709.

Guo Q-H, Sun Y-M, Yu P-M, Hong Z, Lv C-Z. 2007. Norm of auditory verbal learning test in the normal aged in China community. *Chin J Clin Psychol*. 15:132–134.

Hawrylycz MJ, Lein ES, Guillozet-Bongaarts AL, Shen EH, Ng L, Miller JA, van de Lagemaat LN, Smith KA, Ebbert A, Riley ZL et al. 2012. An anatomically comprehensive atlas of the adult human brain transcriptome. *Nature*. 489:391–399.

Jia L, Du Y, Chu L, Zhang Z, Li F, Lyu D, Li Y, Zhu M, Jiao H, Song Y et al. 2020. Prevalence, risk factors, and management of dementia and mild cognitive impairment in adults aged 60 years or older in China: a cross-sectional study. *Lancet Public Health*. 5:e661–e671.

Jie B, Zhang D, Cheng B, Shen D, Alzheimer's Disease Neuroimaging Initiative. 2015. Manifold regularized multitask feature learning for multimodality disease classification. *Hum Brain Mapp*. 36: 489–507.

Jun E, Na KS, Kang W, Lee J, Il SH, Ham BJ. 2020. Identifying resting-state effective connectivity abnormalities in drug-naïve major depressive disorder diagnosis via graph convolutional networks. *Hum Brain Mapp*. 41:4997–5014.

Kingma DP, Ba JL. 2015. Adam: a method for stochastic optimization. In: Bengio Y, LeCun Y. *3rd International Conference on Learning Representations, ICLR 2015 - Conference Track Proceedings*. San Diego (USA): ICLR 2015.

Kipf TN, Welling M. 2017. Semi-supervised classification with graph convolutional networks. In: Bengio Y, LeCun Y. *5th International Conference on Learning Representations, ICLR 2017 - Conference Track Proceedings*. Toulon (France): ICLR 2017.

Kristanto D, Liu M, Liu X, Sommer W, Zhou C. 2020. Predicting reading ability from brain anatomy and function: from areas to connections. *NeuroImage*. 218:116966.

Lawrence AJ, Chung AW, Morris RG, Markus HS, Barrick TR. 2014. Structural network efficiency is associated with cognitive impairment in small-vessel disease. *Neurology*. 83:304–311.

Li X, Zhou Y, Gao S, Dvornek N, Zhang M, Zhuang J, Gu S, Scheinost D, Staib L, Ventola P et al. 2020. BrainGNN: interpretable brain graph neural network for fmri analysis. *Med Image Anal*. 74:102233.

Liang J, Wang S-J, Zhou C. 2021. Less is more: wiring-economical modular networks support self-sustained firing-economical neural avalanches for efficient processing. *Natl Sci Rev*. nwab102.

Linden DEJ. 2012. The challenges and promise of neuroimaging in psychiatry. *Neuron*. 73:8–22.

Liu X, Chen L, Cheng R, Luo T, Lv FJ, Fang W, Gong J, Jiang P. 2019. Altered functional connectivity in patients with subcortical ischemic vascular disease: a resting-state fMRI study. *Brain Res*. 1715:126–133.

Liu M, Zhang H, Shi F, Shen D. 2021. Building dynamic hierarchical brain networks and capturing transient meta-states for early mild cognitive impairment diagnosis. In: de Bruijne M, Cattin PC, Cotin S, Padoy N, Speidel S, Zheng Y, Essert C. *Medical Image Computing and Computer Assisted Intervention - MICCAI 2021 - 24th International Conference, Proceedings*. New York (USA): Springer, p. 574–583.

Lo A, Chernoff H, Zheng T, Lo SH. 2015. Why significant variables aren't automatically good predictors. *Proc Natl Acad Sci U S A*. 112: 13892–13897.

Parisot S, Ktena SI, Ferrante E, Lee M, Guerrero R, Glocker B, Rueckert D. 2018. Disease prediction using graph convolutional networks: application to autism spectrum disorder and Alzheimer's disease. *Med Image Anal*. 48:117–130.

Paszke A, Gross S, Massa F, Lerer A, Bradbury J, Chanan G, Killeen T, Lin Z, Gimelshein N, Antiga L et al. 2019. PyTorch: an imperative style, high-performance deep learning library. In: Wallach HM, Larochelle H, Beygelzimer A, d'Alché-Buc F, Fox EB, Garnett R. *33rd Annual Conference on Neural Information Processing Systems*. Vancouver (Canada). NeurIPS 2019. p. 8026–8037.

Pedregosa F, Varoquaux G, Gramfort A, Michel V, Thirion B, Grisel O, Blondel M, Prettenhofer P, Weiss R, Dubourg V et al. 2011. Scikit-learn: machine learning in Python. *J Mach Learn Res*. 12:2825–2830.

Petersen RC. 2000. Mild cognitive impairment: transition between aging and Alzheimer's disease. *Neurologia*. 15:93–101.

Qiu Y, Yu L, Ge X, Sun Y, Wang Y, Wu X, Xu Q, Zhou Y, Xu J. 2021. Loss of integrity of corpus callosum white matter hyperintensity penumbra predicts cognitive decline in patients with subcortical vascular mild cognitive impairment. *Front Aging Neurosci*. 13:605900.

Roh JH, Lee J-H. 2014. Recent updates on subcortical ischemic vascular dementia. *J Stroke*. 16:18.

Román GC. 2002. Vascular dementia may be the most common form of dementia in the elderly. *J Neurol Sci*. 203:7–10.

Saboksayr SS, Foxe JJ, Wismüller A. 2020. Attention-deficit/hyperactivity disorder prediction using graph convolutional networks. In: Hahn HK, Mazurowski MA. *Medical imaging 2020: computer-aided diagnosis*. Washington (USA): SPIE. Vol. 11314: p. 113141U.

Salvadori E, Poggesi A, Valenti R, Pracucci G, Pescini F, Pasi M, Nannucci S, Marini S, Del Bene A, Ciolli L et al. 2016. Operationalizing mild cognitive impairment criteria in small vessel disease: the VMCI-Tuscany study. *Alzheimers Dement*. 12:407–418.

Schaefer A, Kong R, Gordon EM, Laumann TO, Zuo X-N, Holmes AJ, Eickhoff SB, Yeo BTT. 2018. Local-global parcellation of the human cerebral cortex from intrinsic functional connectivity MRI. *Cereb Cortex*. 28:3095–3114.

Selvaraju RR, Cogswell M, Das A, Vedantam R, Parikh D, Batra D. 2017. Grad-CAM: Visual explanations from deep networks via gradient-based localization. In: O'Conner L. *IEEE International Conference on Computer Vision, ICCV 2017*, Venice (Italy): IEEE Computer Society. p. 618–626.

Shen X, Finn ES, Scheinost D, Rosenberg MD, Chun MM, Papademetris X, Constable RT. 2017. Using connectome-based predictive modeling to predict individual behavior from brain connectivity. *Nat Protoc*. 12:506–518.

Skrobot OA, Black SE, Chen C, DeCarli C, Erkinjuntti T, Ford GA, Kalaria RN, O'Brien J, Pantoni L, Pasquier F et al. 2018. Progress toward standardized diagnosis of vascular cognitive impairment: guidelines from the vascular impairment of cognition classification consensus study. *Alzheimers Dement*. 14:280–292.

Smith EE, Kosslyn SM. 2006. Chapter 6 - working memory. In: Barsalou LW. *Cognitive Psychology: mind and brain*. 1st ed. London (UK): Pearson. p. 239–279.

Song TA, Chowdhury SR, Yang F, Jacobs H, Fakhri GEL, Li Q, Johnson K, Dutta J. 2019. Graph convolutional neural networks for Alzheimer's disease classification. In: Linguraru MG, Grisan E. *Proceedings - International Symposium on Biomedical Imaging, ISBI 2019*. Venice (Italy): IEEE Computer Society. p. 414–417.

Stern Y. 2009. Cognitive reserve. *Neuropsychologia*. 47:2015–2028.

Sui J, Jiang R, Bustillo J, Calhoun V. 2020. Neuroimaging-based individualized prediction of cognition and behavior for mental disorders and health: methods and promises. *Biol Psychiatry*. 88: 818–828.

Sun Y-w, Di QL, Zhou Y, Xu Q, Jun QL, Tao J, Rong XJ. 2011. Abnormal functional connectivity in patients with vascular cognitive impairment, no dementia: a resting-state functional magnetic resonance imaging study. *Behav Brain Res*. 223:388–394.

Ter Telgte A, Van Leijsen EMC, Wiegertjes K, Klijn CJM, Tuladhar AM, De Leeuw FE. 2018. Cerebral small vessel disease: from a focal to a global perspective. *Nat Rev Neurol*. 14:387–398.

Thomas Yeo BT, Krienen FM, Sepulcre J, Sabuncu MR, Lashkari D, Hollinshead M, Roffman JL, Smoller JW, Zöllei L, Polimeni JR et al. 2011. The organization of the human cerebral cortex estimated by intrinsic functional connectivity. *J Neurophysiol*. 106:1125–1165.

Van Essen DC, Felleman DJ. 1991. Distributed hierarchical processing in the primate cerebral cortex. *Cereb Cortex*. 1:1–47.

Van Hoesen GW, Parvizi J, Chu CC. 2000. Orbitofrontal cortex pathology in Alzheimer's disease. *Cereb Cortex*. 10:243–251.

Wang J, Wang L, Zang Y, Yang H, Tang H, Gong Q, Chen Z, Zhu C, He Y. 2009. Parcellation-dependent small-world brain functional networks: a resting-state fmri study. *Hum Brain Mapp*. 30:1511–1523.

Wang Y, Cao W, Sun Y, Chen X, Ding W, Xu Q, Zhou Y, Xu J, Suo S. 2017. White matter integrity in subcortical vascular cognitive impairment: a multimodal structural MRI study. *Curr Alzheimer Res*. 14:991–999.

Wang R, Lin P, Liu M, Wu Y, Zhou T, Zhou C. 2019a. Hierarchical connectome modes and critical state jointly maximize human brain functional diversity. *Phys Rev Lett*. 123:038301.

Wang Y, Tu D, Du J, Han X, Sun Y, Xu Q, Zhai G, Zhou Y. 2019b. Classification of subcortical vascular cognitive impairment using single MRI sequence and deep learning convolutional neural networks. *Front Neurosci*. 13:627.

Wang R, Liu N, Tao YY, Gong XQ, Zheng J, Yang C, Yang L, Zhang XM. 2020. The application of rs-fMRI in vascular cognitive impairment. *Front Neurol*. 11:951.

Wang Z, Goerlich KS, Ai H, Aleman A, Luo YJ, Xu P. 2021a. Connectome-based predictive modeling of individual anxiety. *Cereb Cortex*. 31:3006–3020.

Wang R, Liu M, Cheng X, Wu Y, Hildebrandt A, Zhou C. 2021b. Segregation, integration, and balance of large-scale resting brain networks configure different cognitive abilities. *Proc Natl Acad Sci U S A*. 118:e2022288118.

Wee CY, Liu C, Lee A, Poh JS, Ji H, Qiu A. 2019. Cortical graph neural network for AD and MCI diagnosis and transfer learning across populations. *NeuroImage Clin*. 23:101929.

Whelan R, Garavan H. 2014. When optimism hurts: inflated predictions in psychiatric neuroimaging. *Biol Psychiatry*. 75:746–748.

Winblad B, Palmer K, Kivipelto M, Jelic V, Fratiglioni L, Wahlund LO, Nordberg A, Bäckman L, Albert M, Almkvist O et al. 2004. Mild cognitive impairment - beyond controversies, towards a consensus: report of the International Working Group on mild cognitive impairment. *J Intern Med*. 256:240–246.

Xing X, Li Q, Yuan M, Wei H, Xue Z, Wang T, Shi F, Shen D. 2021. DS-GCNs: connectome classification using dynamic spectral graph convolution networks with assistant task training. *Cereb Cortex*. 31:1259–1269.

Yan C-G, Zang Y-F. 2010. DPARSF: a MATLAB toolbox for "pipeline" data analysis of resting-state fMRI. *Front Syst Neurosci*. 4:13.

Ye Q, Bai F. 2018. Contribution of diffusion, perfusion and functional MRI to the disconnection hypothesis in subcortical vascular cognitive impairment. *Stroke Vasc Neurol*. 3:e000080.

Yi L, Wang J, Jia L, Zhao Z, Lu J, Li K, Jia J, He Y, Jiang C, Han Y. 2012. Structural and functional changes in subcortical vascular mild cognitive impairment: a combined voxel-based morphometry and resting-state fMRI study. *PLoS One*. 7:e44758.

Yi LY, Liang X, Liu DM, Sun B, Ying S, Yang DB, Bin LQ, Jiang CL, Han Y. 2015. Disrupted topological Organization of Resting-State Functional Brain Network in subcortical vascular mild cognitive impairment. *CNS Neurosci Ther*. 21:846–854.

Zalesky A, Fornito A, Harding IH, Cocchi L, Yücel M, Pantelis C, Bullmore ET. 2010. Whole-brain anatomical networks: does the choice of nodes matter? *NeuroImage*. 50:971–983.

Zhang HY, Wang SJ, Liu B, Ma ZL, Yang M, Zhang ZJ, Teng GJ. 2010. Resting brain connectivity: changes during the progress of Alzheimer disease. *Radiology*. 256:598–606.

Zhang Y, Zhang H, Chen X, Lee SW, Shen D. 2017. Hybrid high-order functional connectivity networks using resting-state functional MRI for mild cognitive impairment diagnosis. *Sci Rep*. 7: 1–15.

Zhou X, Hu X, Zhang C, Wang H, Zhu X, Xu L, Sun Z, Yu Y. 2016. Aberrant functional connectivity and structural atrophy in subcortical vascular cognitive impairment: relationship with cognitive impairments. *Front Aging Neurosci*. 8:14.